International Journal of Engineering Trends and Technology
ISSN: 2231–5381 / https://doi.org/10.14445/22315381/IJETT-V73I11P118

Volume 73 Issue 11, 252-260, November 2025

Original Article

Power Generation of a Hinged Arm WEC

Gustavo O. Guarniz Avalos

Faculty of Engineering, Universidad Tecnológica del Perú, Lima, Peru.

Corresponding Author : gguarniz@utp.edu.pe

Received: 25 June 2024 Revised: 15 October 2024 Accepted: 18 October 2024 Published: 25 November 2025

Abstract *- Waves contain substantial renewable energy potential; however, their capture presents a significant challenge. Electricity generation capability relies on the effectiveness of the process that converts ocean wave motion into usable power. The direct drive system provides high efficiency; however, the gearbox is an essential element in this system to achieve the desired performance. This research is intended to evaluate the energy performance of an articulated arm Wave Energy Converter (WEC) with a point absorber. The system is mainly distinguished by a pulley system for energy transformation, which influences the transmission ratio. The methodology used to examine the device hydrodynamically is linear wave theory, which introduces viscous damping. Regular waves between 1 m and 2 m in height and 10s to 14s in period, a gearbox with a ratio of up to 40, and a generator rated power between 23kW and 96 kW are analyzed in terms of energy efficiency. The analysis suggests that the mean power increases as the interval between waves shortens and their amplitude grows. However, when both the wave period and height decrease, the capture width ratio increases. The maximum mean performance for the generators reaches nearly half of their nominal rating. To obtain the described performance, the gearbox transmission ratio varies between 8 and 22. The findings indicate that the device shows good performance in such rough seas, and such high gear ratios are not necessary.*

Keywords *- Direct mechanical drive PTO, Pulley system, WEC, Gearbox transmission ratio.*

1. Introduction

Renewable energies emerge as the forefront alternative, playing a pivotal role in mitigating the adverse impacts associated with the use of fossil fuels. The transition stands as a crucial step towards achieving sustainability and combating climate change [1, 2]. Marine energy emerges as the most abundant renewable source, offering the potential to fulfill the global electricity demand [3]. Wave energy production exhibits greater constancy and predictability [4, 5], and it offers a glimpse into how it will significantly contribute to a more sustainable world. In search of sustainable and renewable energy, the appeal of harnessing the kinetic energy present in ocean waves has led WECs to develop innovative solutions; the global development of this device technology is booming [6]. The point absorber, being of compact size, minimal complexity, and cost-effectiveness, stands out as the most extensively researched type of wave energy converter [5, 7-9]. It has the ability to simultaneously harvest gravitational and wave energy [10]. The small dimensions of the point absorber compared to the wavelength mean that the point absorber effectively harnesses energy from waves coming from all directions [11, 12]. Wave energy converters with an articulated arm connecting the point absorber to the coast are gaining attention for their straightforward installation and maintenance, which contributes to their overall viability and sustainability [13]. The Power Take-Off (PTO), which is similar to the brain because it converts the floating body's kinetic energy into electrical energy, is an essential component of the WEC [8]. It has the capacity to optimize energy capture. Among major power take-offs, the efficiency of hydraulic and pneumatic systems can be lower compared to other systems due to energy losses during fluid transmission and conversion processes [6]. Additionally, hydraulic and pneumatic systems typically require meticulous maintenance. Oil leaks from hydraulic converters are common; they can cause pollution to the environment [5]. In recent decades, the adoption of Direct Drive Mechanical Systems (DDMS) and Direct Electrical Drive Systems (DEDS) has shown an increase [8]. A total of 31 developers worldwide employ DDMS, making it the most widely used, and the hydraulic turbine is in second place with 21 developers [6]. DEDS exhibits enhanced efficiency; However, it is noteworthy that the velocity of the linear generator is currently low [6], and efforts to address this challenge are still ongoing in research [14]. The air gap configuration constitutes an additional disadvantage in the design of this type of device [15]. DDMS can be made up of components such as unidirectional bearings, rack and pinion, pulley systems, belt drive systems, or screw mechanisms [16-19]. They have been widely used in industry. On the other hand, moving parts are subject to wear over time, which can affect the reliability and efficiency of the system, necessitating regular maintenance. This system is exposed to high load cycles [6].

A clear example is the rack and pinion mechanism, which has been extensively studied experimentally in WECs [16, 20-22], and has inspired patents with a very simplified operating concept, such as [23]. The problem is their comparatively short lifespan [24]. But there is no doubt that it always provides high efficiency, reaching 97% [25]. A key feature of DDMS is the three energy conversions, which lead to high energy generation efficiency [26]. Because it affects the cost, it is noted that wave energy converter maintenance will always be a topic of concern. However, the most important challenge is the reliability of the device's performance [27, 28]. The technological maturity has not been reached, and the price of wave energy cannot yet compete with more established alternatives such as solar or wind power [29]. Device reliability can reduce this existing cost gap.

Designing, operating, and installing WECs are more complex than land-based structures due to harsh marine conditions. They must withstand extreme operational and climatic loads, as well as resist seawater corrosion. Offshore maintenance is expensive and risky, so efficient maintenance planning is crucial. On the other hand, coastal WECs offer easier access but must compete with other shoreline uses unless integrated into existing structures to reduce costs [30], [31]. According to [32, 33] hinged arm WECs show a great advantage in terms of installation, maintenance, and protection in rough seas.

Additionally, WECs contribute to the accumulation of coastal silt and lessen marine erosion; as a result, their effectiveness in producing electricity is justified, as are the economic and environmental advantages that result from protecting the coast [34]. This study aims to study the performance of an articulated arm WEC using a DDMS. Using a pulley system is a feature of this articulated arm WEC instead of a hydraulic system widely used in this type of WEC, which provides lower efficiency [6]. The analysis focuses on evaluating the behavior of the PTO system in power generation. The study incorporates regular waves with different heights and periods. Three permanent magnet generators and the transmission ratio of the gearbox are also considered.

2. The WEC Description

Figure 1 depicts the representative model of the hinged arm energy device studied. The diameter and draft of the point absorber are 5m and 2m, and its mass is equal to 40.25t. The articulated arm length is 10m, the variables h_1, h_2, and h_3 take the value of 3.83m, and the mass of the counterweight is equal to 0.25t. Figure 2 shows the PTO system's constituent parts. The unidirectional bearing and pulley system converts the point absorber's oscillatory action into one-way rotational motion. Through the use of a gearbox, the rotating motion accelerates and powers an electrical generator. The kinetic energy that is captured is stored in a flywheel.

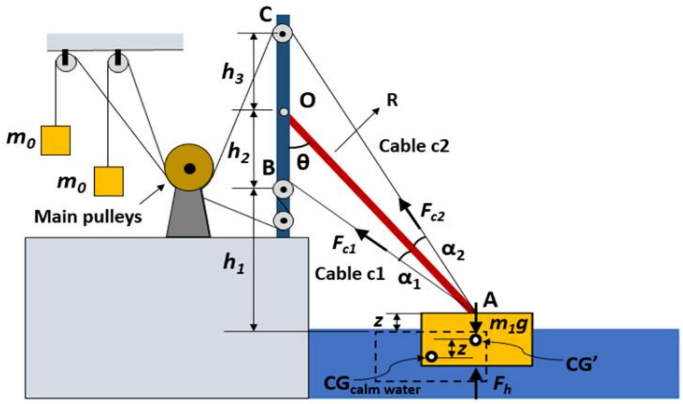

Fig. 1 Schematic model of WEC

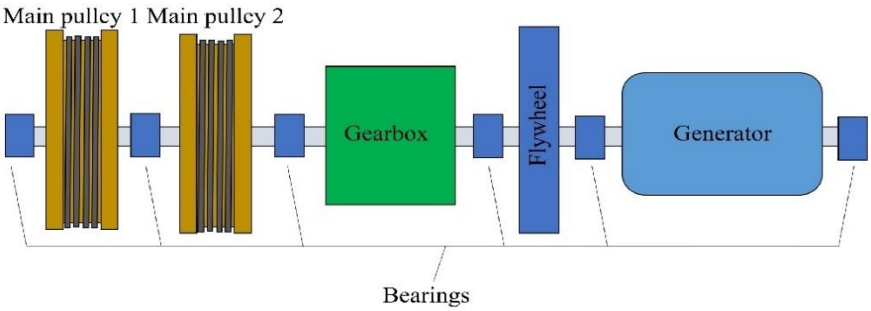

Fig. 2 Components of the PTO system

3. Equation of Motion

Based on Figure 1, the assumption is made that the buoy maintains a constant vertical position, which is consistent with references [35, 36]. Equation 1 describes how the buoy oscillates around the point O.

$$-m_1 gRsen\theta + F_h Rsen\theta - F_{c1} Rsen\alpha_1 + F_{c2} Rsen\alpha_2 = J\ddot{\theta} \quad (1)$$

Where J is the moment inertia of the floating body, $\ddot{\theta}$ is the angular acceleration, m_1 is the mass of the buoy, g is the acceleration of gravity, F_{c1} and F_{c2} are the tensions of the cables, F_h is the net force by water, which is always considered as a vertical force. This is discussed in Section 4, where R is the distance $\overline{OA}$, the angles α_1 and α_2 are shown in Figure 1.

In Figure 1, the distances between points A and B and the points A to C are defined in Equations 2 and 3, respectively. The relation of these distances and the velocity of the pulleys 1 and 2 is defined in Equations 4 and 5, respectively. The horizontal projection of the length R is shown in Equation 6, which depends on the z displacement of the buoy. According to Figure 1, the buoy is regarded as keeping a constant vertical position, which is consistent with references [19-22]. Equation 1 describes the movement of the buoy around the point O.

$$L_1 = [R^2 + h_2^2 - 2Rh_2 cos\theta]^{1/2} \quad (2)$$

$$L_2 = [R^2 + h_3^2 - 2Rh_3 \cos(\pi - \theta)]^{1/2} \quad (3)$$

$$\dot{L}_1 = \dot{\delta}_1 r \quad (4)$$

$$\dot{L}_2 = \dot{\delta}_2 r \quad (5)$$

$$Rcos\theta = (h_1 + h_2 - z) \quad (6)$$

4. Hydrodynamic Force

The calculation of hydrodynamic forces employs the linear theory of waves. The propagation of the waves is perpendicular to the view in Figure 1; the oscillation of the floating body arises exclusively from the action of the waves in the vertical direction. In the linear theory, viscous damping is taken into account, and the total force is expressed in Equation 7.

$$\boldsymbol{F_h = F_v + F_b + F_r + F_e} \quad (7)$$

Where F_v is the viscous damping force, F_e is the wave excitation force, F_r is the wave radiation force and F_b is the buoyance force. This study exclusively focuses on regular waves, whose elevation is delineated by Equation 8, which depends on the amplitude and the angular frequency $A_{w,}$ and ω, respectively, of the wave.

$$z_w = A_w cos(\omega t) \quad (8)$$

The restoring force F_{rs} is formulated as the combined effects of gravity and buoyancy forces, and it is defined by the displacement z and the hydrostatic stiffness coefficient c_{33} of the point absorber, as shown in Equation 9.

$$F_{rs} = F_b - m_1 g = -c_{33} z \quad (9)$$

The force of radiation is determined in accordance with [37], which uses the convolution integral formulation, see Equation 10. It depends on the retardation function K_r and the added mass a_∞.

$$F_r = -a_\infty \ddot{z} - \int_0^t K_r(t-\tau)\dot{z}(\tau)\, d\tau \quad (10)$$

According to [38], the calculation of K_r is determined in Equation 11, which depends on the damping coefficient b_{33}.

$$K_r(t) = \frac{2}{\pi}\int_0^\infty b_{33}(\omega)\cos(\omega t)\, d\omega \quad (11)$$

The force F_e is defined in Equation 12.

$$F_e = \frac{H}{2} F_{33} \cos(\omega t - \phi_{33}) \quad (12)$$

Where the wave height is H, the force amplitude of the wave is F_{33} and ϕ_{33} is the wave force phase shift. The point absorber considered in this study corresponds to study; therefore, the hydrodynamic coefficients are extracted from this research and were obtained using ANSYS/AQWA. The force due to the viscous effect is determined as outlined in [25], see Equation 13.

$$F_v = -\frac{1}{2}\rho C_d A(\dot{z} - u)|\dot{z} - u| \quad (13)$$

Where u and $\dot{z}$ are the fluid velocity and the body velocity, respectively, and the water density is ρ, C_d is the coefficient of drag, and A represents the buoy's cross-sectional area. C_d of the buoy studied is 1.85, C_d was calculated through a decay test, based on the linear potential theory and the viscous effect, several values of C_d were analyzed to reproduce the decay test.

5. PTO System

In Figure 2, the slipping of the cable on the pulleys is not considered. The dynamic of the pulley 1 is described in Equation 14; only the generator shaft bearing torque is considered. When the electric generator and the buoy are disconnected, Equation 14 is replaced by Equation 15. The counterweight movement corresponding to pulley 1 is formulated using Equation 16. The equations for the main pulley 2 are shown in Equations 17 to 19.

$$[J_1 + c^2 J_2]\ddot{\delta}_1 = F_{c1}r - F_{c01}r - \left[c\left(T_g + 3T_b\right)\right] \quad (14)$$

$$J_1\ddot{\delta}_1 = F_{c1}r - F_{c01}r \quad (15)$$

$$m_0\ddot{\delta}_1 r = F_{c01} - m_0 g \quad (16)$$

$$[J_1 + c^2 J_2]\ddot{\delta}_2 = F_{c2}r - F_{c02}r - \left[c\left(T_g + 3T_b\right)\right] \quad (17)$$

$$J_1\ddot{\delta}_2 = F_{c2}r - F_{c02}r \quad (18)$$

$$m_0\ddot{\delta}_2 r = F_{c02} - m_0 g \quad (19)$$

Where the inertia of the gearbox, the shaft, and the main pulley is represented by J_1. Regarding the flywheel, the generator, and its shaft, the inertia is represented by J_2; $\ddot{\delta}_1$ and $\ddot{\delta}_2$ are the mean pulleys' angular acceleration, c is the transmission ratio, r is the radius of the pulleys, which is equivalent to 0.15m, T_g and T_b are the torques of the generator and each generator shaft bearing, see Figure 2; the cable tensions F_{c01} and F_{c02} support each counterweight. Three permanent magnet electric generators, G1, G2, and G3, are evaluated, and have a rated power of 23 kW, 77kW, and 96kW, respectively. G1 and G2 have a rated speed of 400 rpm and G3 of 350 rpm, details in [39]. The curves of power are depicted in Figure 3. Its torque is determined using Equation (20).

$$T_g = P_g\,/(\eta_g \omega_g) \quad (20)$$

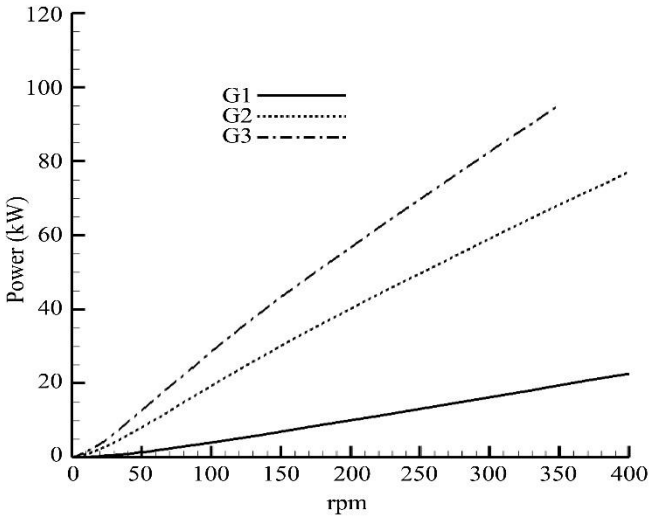

Fig. 3 Power curves of G1, G2, and G3

Where ω_g, η_g and P_g are the speed, efficiency, and power of the electric generator. Each bearing's torque is determined using the Petroff equation described in [40]. The electric generator and the buoy are connected when Equation 21 or Equation 22 is satisfied, ω_g takes the value of $c\dot{\delta}_1$or $c\dot{\delta}_2$.

$$\omega_g < c\dot{\delta}_1 \quad (21)$$

$$\omega_g < c\dot{\delta}_2 \quad (22)$$

If the generator's speed range is being maintained, Equation 23 determines the generator speed in the event that the coupling does not occur. Otherwise, for this instant of time t, the generator shaft speed is governed by Equation 24.

$$\omega_g(t + \Delta t) = \omega_g(t) - \frac{(T_g + 3T_b)}{J_2}\Delta t \quad (23)$$

$$\omega_g(t + \Delta t) = \omega_g(t) - \frac{3T_b}{J_2}\Delta t \quad (24)$$

Where Δt is the time step.

The average power P_m is calculated using Equation 25.

$$P_m = \frac{1}{T}\int_0^T P_g\ dt \quad (25)$$

Where, P_g denotes the generated electrical power over the time period T. The time series is obtained by carrying out over a period of 2000 seconds; the initial 1000 seconds are not considered to eliminate the transient response. The Capture Width Ratio (CWR) is defined by Equation 26.

$$CWR = \frac{P_m}{P} \quad (26)$$

Where the power of the incident wave P is defined in Equation (27).

$$P = \frac{1}{8}\rho g {H_w}^2 c_g D \quad (27)$$

Where H_w represents the height wave, c_g denotes the group velocity and D is the buoy's diameter.

6. Results and Discussion

Below is shown the production of power considering the height (Hw) and the period (Tp) of the wave, the nominal power of each generator, and the gear ratio of the gearbox. All these variables have a constant value to calculate the mean power according to Equation 5. This study examines regular waves, specifically focusing on the characteristics of the Peruvian sea as outlined in [41]. Regarding the transmission ratio, since this variable increases the inertia and torque in the system in a quadratic and linear manner (see Equations 14 and 17), the analysis considers the influence of this variable on power generation.

6.1. Analysis of the Average Electrical Power

Figure 4 illustrates the average power in a period of 12 s for three wave heights. A rise and a fall in the power is observed, revealing an ideal value for the transmission ratio. Notably, the changes in power are not characterized by a smooth transition; it is more irregular near the maximum

power, and the power decreases faster, showing in some cases an irregular behavior. The best values of power registered for each generator are around 38.5 kW, 32.5 kW, and 9.5kW, which correspond to G3, G2, and G1, respectively. It is noteworthy that in all cases, the WEC fails to generate power at certain gear ratio values. As the wave height grows, the absence of power generation commences at lower gear ratio values. For all generators, the change in maximum average power is only marginally affected by wave height, with the greatest value occurring at 2.0 m. Conversely, the wave height diminishes the optimal gear ratio across all generators. Varying Hw from 1 to 2 meters reduces the optimum gear ratio value by approximately half. G3 demonstrates superior power production performance. Generally, for a given wave height, the duration of non-production of power is slightly shorter when the generator's rated power is lower.

Figure 5 illustrates power production under a 1.5 m wave condition for three wave periods. Similar to the previous figure, an optimal gear ratio is evident, and the power variation is characterized by non-smooth transitions with respect to the gear ratio. Notably, this second analysis's maximum power is larger than the first, reaching around 44 kW, 37 kW, and 11kW for G3, G2, and G1, respectively. The absence of energy production is influenced by the decrease in wave period. When comparing the same generator, a reduction in wave period from 14 seconds to 10 seconds leads to a rise in maximum power, as well as a decline in the optimal gear ratio. However, this decrease in the optimal gear ratio is less pronounced compared to the reduction caused by changes in wave height in Figure 4. A decrease from 14s to 12s wave period generally leads to a decrease or nearly identical maximum power, with exceptions observed for specific generators. Once again, the G3 generator stands out for its superior power generation output compared to others. For every generator, the highest power obtained surpasses that seen in Figure 4.

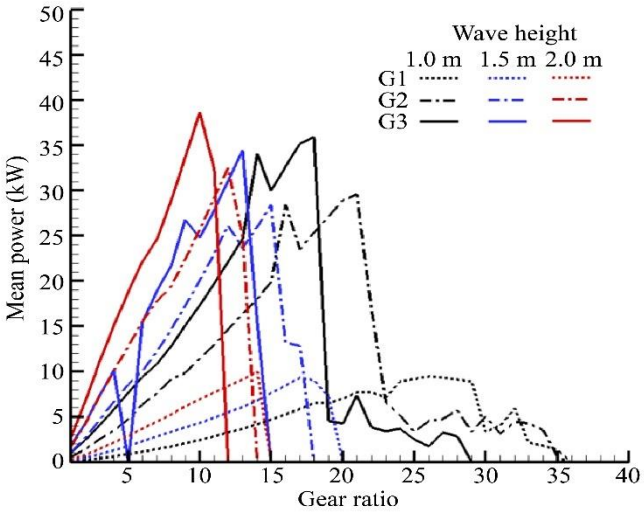

Fig. 4 Average power at Tp = 12s

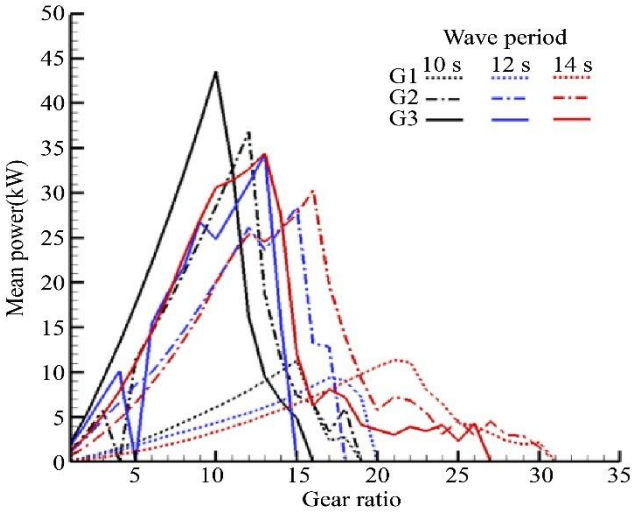

Fig. 5 Average power at Hw = 1.5 m

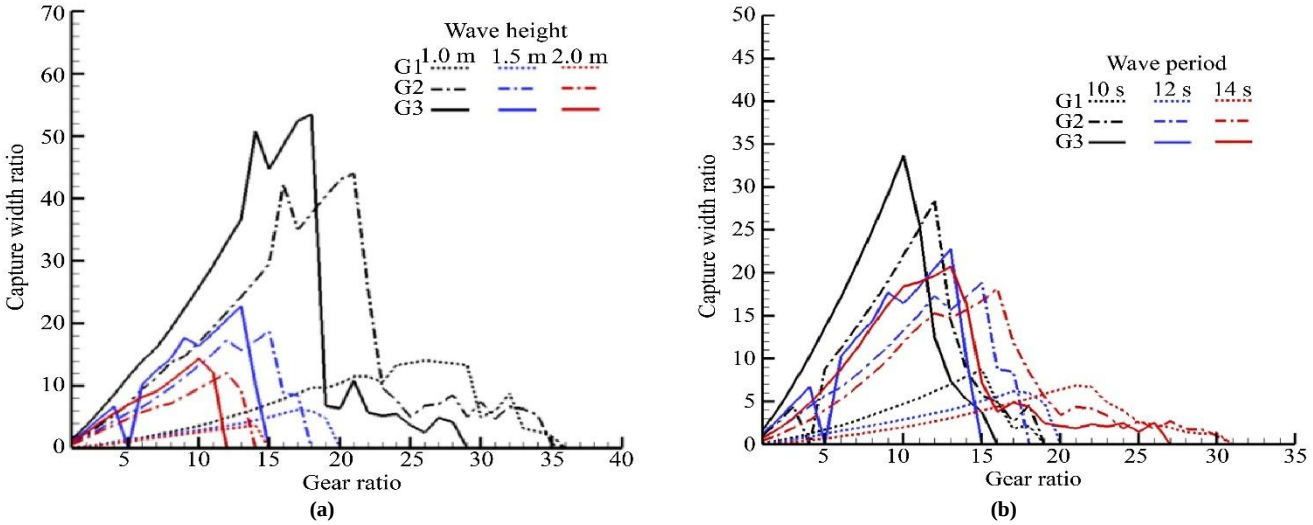

Fig. 6 CWR of WEC (a) Wave period Tp = 12s, and (b) Wave height Hw =1.5m.

6.2. CWR of the WEC

In Figure 6, the results show that the CWR increases with the reduction of the height and period. The height's influence is greater than the period. In Figure 6(a), generators G3 and G2 show the best CWR value, 53% and 44%, respectively; the maximum CWR of the rest does not exceed 23%.

For the G3 generator, the range of gear ratios to obtain a CWR greater than 30% is between 12 and 18, and for the G2 generator, it is between 16 and 21. In Figure 6(b), all cases show a CWR less than 35%; the G3 and G2 generators are the only ones that exceed a CWR of 25% and are obtained for a gear ratio of 10 and 12, respectively. The G1 generator shows the lowest CWR values, generally less than 10%.

6.3. Time Series of WEC Performance

Figure 7 provides the time-dependent response at the maximum CWR obtained in Figure 6(a), 53%. Figure 7(a) shows that the amplitude in upward movement does not exceed 0.5m, and in the downward movement does not exceed 1 m; the speed of the buoy does not exceed 0.6 m/s. In Figure 7(b), discrete points represent the generator speed, illustrating the connecting and disconnecting dynamics between the electric generator and the buoy. The generator speed shows that the power production occurs always, except at one point in time of each oscillation (black dot), the generator shuts down because the rated velocity of the electric generator is exceeded. In Figure 7(c), power production is solely driven by the point absorber when its velocity experiences an increase in the downward movement; the remaining duration experiences power generation, attributed to the point absorber or flywheel. The power production is greater in the downward movement; the maximum power is about 95 kW, which is practically the rated power of the G3 generator. The torque shows an almost constant value over time of 2.9kNm and rapidly decreases and increases as the velocity of the buoy crosses zero. Power and torque take a value of zero when the generator is off, see Figure 7(b) (black dot).

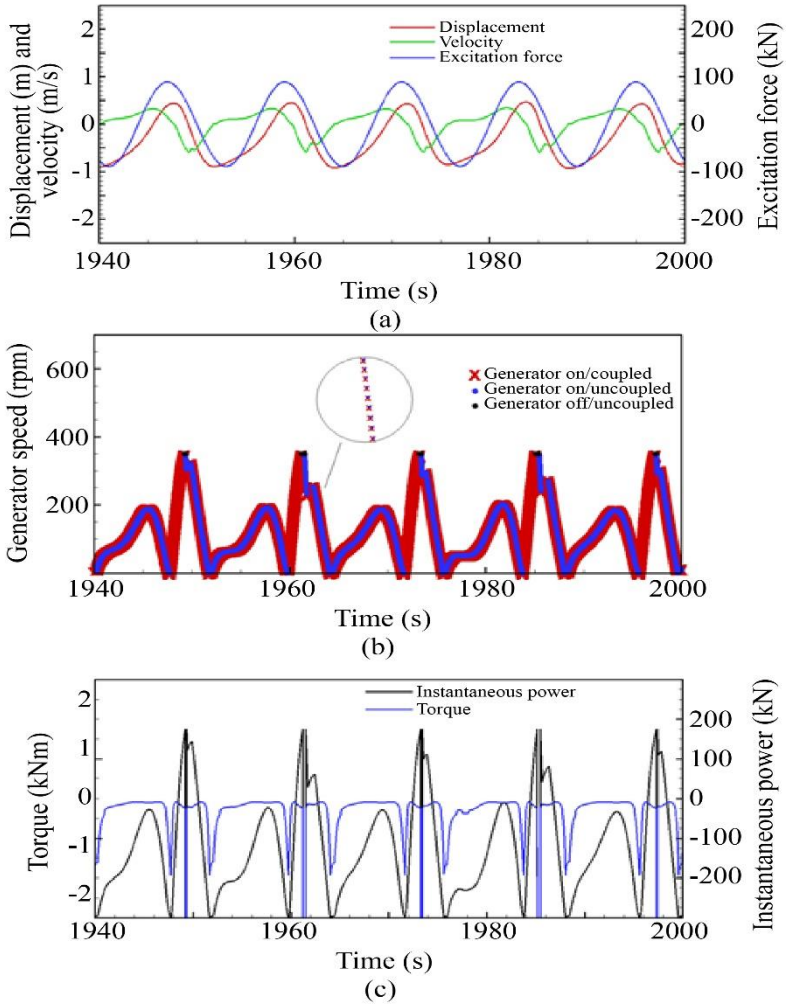

Fig. 7 WEC performance for G3, Tp = 12 s, c = 18, and Hw = 1 m

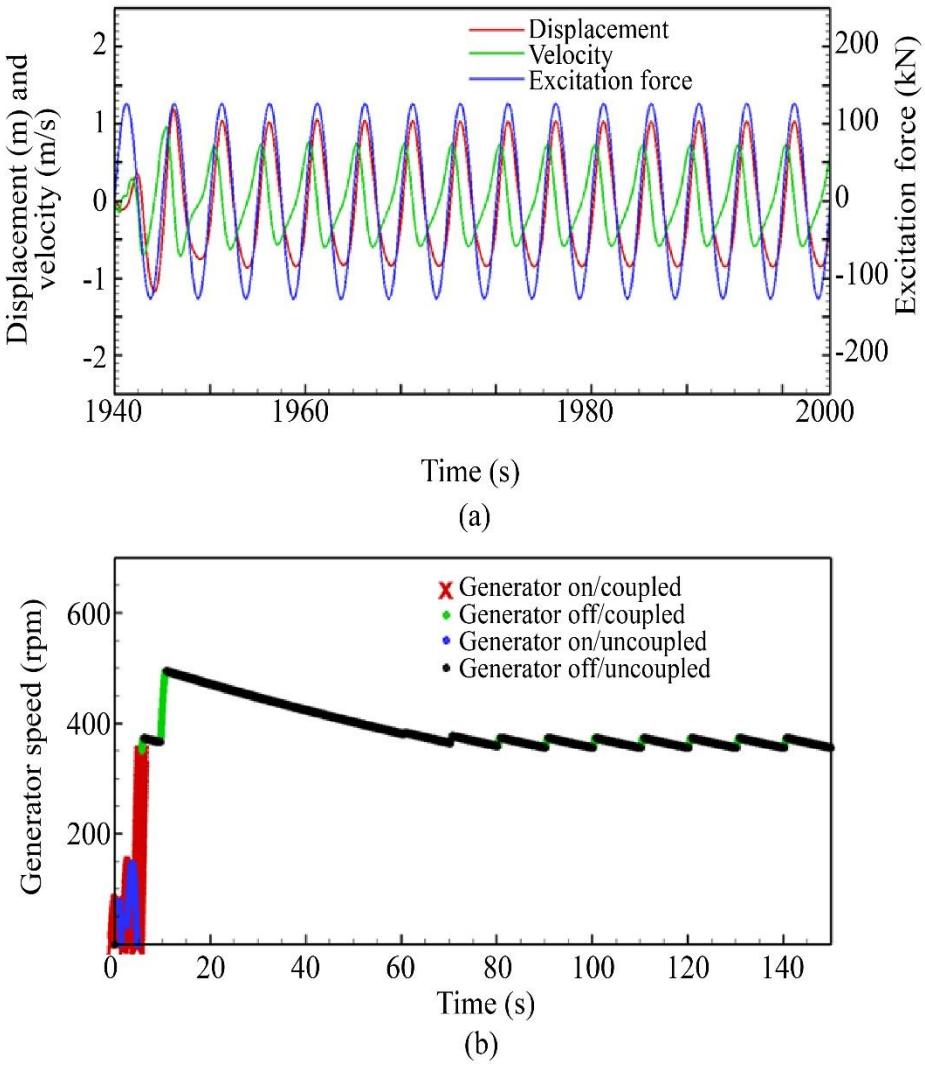

Fig. 8 Times series of WEC for G3, wave period = 10 s, wave height = 1.5 m, gear ratio = 16

The time series in Figure 8 is explained because zero power is observed in Figures 4 and 5. During the first 5s, power generation occurs through the connecting and disconnecting of the PTO system. After this time, the generator is operating faster than its rated speed, the PTO system engages but does not produce power (green dot), then the PTO is uncoupled, and the speed decreases (black dot) according to Equation 24. This behavior is repeated several times until reaching the steady state without energy production. Therefore, the point absorber oscillates practically free after the first 5 s, the maximum amplitude of displacement and velocity is approximately 1 m and 0.7 m/s, respectively. The exciting force and the velocity show lag all the time.

7. Conclusion

The performance of the proposed WEC incorporates generators with rated powers of 23 kW, 77 kW, and 96 kW. The effect of the gearbox ratio and the characteristics of the wave are also examined. Key conclusions drawn from the analysis indicate that the reduction of wave period and the increase of wave height increase the mean power. When both wave parameters decrease, the CWR of the WEC increases; However, wave height has a bigger impact than wave period. The generators labeled as G3 and G2 show higher CWR; the maximum CWR obtained is 53% and 44%, respectively. To obtain these values, the transmission ratio does not exceed 18. In certain instances, PTO engagement causes the generator speed to exceed the operating range, resulting in the production of null power. Thanks to the flywheel, the WEC produces energy when the buoy and the electric generator are disconnected, smoothing the energy generated over time. In future work, the performance of the WEC will be analyzed in irregular waves to obtain a realistic behavior of the efficiency of the device.

Acknowledgments

The author acknowledges the support from Universidad Tecnológica del Perú.

References

[1] M. Unsal Sasmaz et al., "The Relationship between Renewable Energy and Human Development in OECD Countries: A Panel Data Analysis," *Sustainability*, vol. 12, no. 18, pp. 1-16, 2020. [CrossRef] [Google Scholar] [Publisher Link]

[2] Oluwasegun B. Adekoya, Joshua K. Olabode, and Syed K. Rafi, "Renewable Energy Consumption, Carbon Emissions and Human Development: Empirical Comparison of the Trajectories of World Regions," *Renewable Energy*, vol. 179, pp. 1836-1848, 2021. [CrossRef] [Google Scholar] [Publisher Link]

[3] Yuanrui Sang et al., "Ocean (Marine) Energy," *Comprehensive Energy Systems*, vol. 1, pp. 733-769, 2018. [CrossRef] [Publisher Link]

[4] Alicia Terrero González et al., "Is Wave Energy Untapped Potential?," *International Journal of Mechanical Sciences*, vol. 205, 2021. [CrossRef] [Google Scholar] [Publisher Link]

[5] Iraide López et al., "Review of Wave Energy Technologies and the Necessary Power-Equipment," *Renewable and Sustainable Energy Reviews*, vol. 27, pp. 413-434, 2013. [CrossRef] [Google Scholar] [Publisher Link]

[6] Raju Ahamed, Kristoffer McKee, and Ian Howard, "Advancements of Wave Energy Converters based on Power Take Off (PTO) Systems: A Review," *Ocean Engineering*, vol. 204, 2020. [CrossRef] [Google Scholar] [Publisher Link]

[7] Scott J. Beatty et al., "Experimental and Numerical Comparisons of Self-Reacting Point Absorber Wave Energy Converters in Irregular Waves," *Ocean Engineering*, vol. 173, pp. 716-731, 2019. [CrossRef] [Google Scholar] [Publisher Link]

[8] Marcos Blanco et al., *Recent Advances in Direct-Drive Power Take-OFF (DDPTO) Systems for Wave Energy Converters based on Switched Reluctance Machines (SRM)*, Ocean Wave Energy Systems, pp. 487-532, 2022. [CrossRef] [Google Scholar] [Publisher Link]

[9] Bingyong Guo et al., "A Review of Point Absorber Wave Energy Converters," *Journal of Marine Science and Engineering*, vol. 10, no. 10, pp. 1-37, 2022. [CrossRef] [Google Scholar] [Publisher Link]

[10] Date Li et al., "Analysis of Floating Buoy of a Wave Power Generating Jack-Up Platform Haiyuan 1," *Advances in Mechanical Engineering*, vol. 2013, 2013. [CrossRef] [Google Scholar] [Publisher Link]

[11] Athanasios Kolios et al., "Reliability Assessment of Point-Absorber Wave Energy Converters," *Ocean Engineering*, vol. 163, pp. 40-50, 2018. [CrossRef] [Google Scholar] [Publisher Link]

[12] Jingjin Xie, and Lei Zuo, "Dynamics and Control of Ocean Wave Energy Converters," *International Journal of Dynamics and Control*, vol. 1, no. 3, pp. 262-276, 2013. [CrossRef] [Google Scholar] [Publisher Link]

[13] Alberto Albert et al., "Mechanical Design and Simulation of an Onshore Four-Bar Wave Energy Converter," *Renewable Energy*, vol. 114, pp. 766-774, 2017. [CrossRef] [Google Scholar] [Publisher Link]

[14] Zhenwei Liu et al., "A Study of a Speed Amplified Linear Generator for Low-Frequency Wave Energy Conversion," *Mechanical Systems and Signal Processing*, vol. 149, 2021. [CrossRef] [Google Scholar] [Publisher Link]

[15] M.A. Mueller, and N.J. Baker, "Direct Drive Electrical Power Take-Off for Offshore Marine Energy Converters," *Proceedings of the Institution of Mechanical Engineers, Part A: Journal of Power and Energy*, vol. 219, no. 3, pp. 223-234, 2005. [CrossRef] [Google Scholar] [Publisher Link]

[16] P.C. Binh et al., "Analysis, Design and Experiment Investigation of a Novel Wave Energy Converter," *IET Generation, Transmission and Distribution*, vol. 10, no. 2, pp. 460-469, 2016. [CrossRef] [Google Scholar] [Publisher Link]

[17] Jens Peter Kofoed et al., "Real Sea Testing of a Small Scale Weptos WEC Prototype," *Proceedings of the International Conference on Offshore Mechanics and Arctic Engineering - OMAE*, Madrid, Spain, vol. 10, pp. 1-9, 2018. [CrossRef] [Google Scholar] [Publisher Link]

[18] Masayuki Sanada, Yukinori Inoue, and Shigeo Morimoto, "Generator Design and Characteristics in Direct-Link Wave Power Generating System Considering Appearance Probability of Waves," *2012 International Conference on Renewable Energy Research and Applications, ICRERA 2012*, Nagasaki, Japan, pp. 1-6, 2012. [CrossRef] [Google Scholar] [Publisher Link]

[19] Jonas Sjolte et al., "Exploring the Potential for Increased Production from the Wave Energy Converter Lifesaver by Reactive Control," *Energies*, vol. 6, no. 8, pp. 3707- 3733, 2013. [CrossRef] [Google Scholar] [Publisher Link]

[20] S. Chandrasekaran, and B. Raghavi, "Design, Development and Experimentation of Deep Ocean Wave Energy Converter System," *Energy Procedia*, vol. 79, pp. 634-640, 2015. [CrossRef] [Google Scholar] [Publisher Link]

[21] Wei Peng et al., "Experimental and Numerical Study on Hydrodynamic Performance of a Wave Energy Converter using Wave-Induced Motion of Floating Body," *Journal of Renewable and Sustainable Energy*, vol. 7, no. 5, 2015. [CrossRef] [Google Scholar] [Publisher Link]

[22] H. Ming Chen, and Donald R. DelBalzo, "Electromagnetic Spring for Sliding Wave Energy Converter," *OCEANS 2015 - MTS/IEEE Washington*, Washington, DC, USA, 2016. [CrossRef] [Google Scholar] [Publisher Link]

[23] Joseph P. La Stella, and Michael G. Tornabene, "Ocean Wave Energy Device," *US4599858A*, 1977. [Publisher Link]

[24] Markel Penalba, and John V. Ringwood, "A Review of Wave-to-Wire Models for Wave Energy Converters," *Energies*, vol. 9, no. 7, pp. 1-45, 2016. [CrossRef] [Google Scholar] [Publisher Link]

[25] Miriam Metcalfe, Gearing Up for Efficiency, Gear Solution, 2025. [Online]. Available: https://gearsolutions.com/features/gearing-up-for-efficiency/

[26] Arthur Pecher, and Jens Peter Kofoed, *Handbook of Ocean Wave Energy*, 1st ed., Springer Cham, 2017. [CrossRef] [Google Scholar] [Publisher Link]
[27] Hai Li et al., "Advanced Wave Energy Conversion Technologies for Sustainable and Smart Sea: A Comprehensive Review," *Renewable Energy*, vol. 238, 2025. [CrossRef] [Google Scholar] [Publisher Link]
[28] Wanan Sheng, "Wave Energy Conversion and Hydrodynamics Modelling Technologies: A Review," *Renewable and Sustainable Energy Reviews*, vol. 109, pp. 482-498, 2019. [CrossRef] [Google Scholar] [Publisher Link]
[29] Tunde Aderinto, and Hua Li, "Review on Power Performance and Efficiency of Wave Energy Converters," *Energies*, vol. 12, no. 22, pp. 1-24, 2019. [CrossRef] [Google Scholar] [Publisher Link]
[30] Yingpeng Cai, and Enze Li, "Technology, Geometry, Performance and Challenges in Wave Energy Converters," *4th International Conference on Mechanical Engineering, Civil Engineering and Material Engineering (MECEME 2023)*, vol. 52, pp. 105-118, 2023. [CrossRef] [Google Scholar] [Publisher Link]
[31] Tunde Aderinto, and Hua Li, "Ocean Wave Energy Converters: Status and Challenges," *Energies*, vol. 11, no. 5, pp. 1-26, 2018. [CrossRef] [Google Scholar] [Publisher Link]
[32] Who We Are, Eco Wave Power, 2025. [Online]. Available: https://www.ecowavepower.com/about/who-are-we/
[33] Wave Star, Unlimited Clean Energy, 2025. [Online]. Available: https://wavestarenergy.com/
[34] Mehrdad Moradi, Narimene Chertouk, and Adrian Ilinca, "Modelling of a Wave Energy Converter Impact on Coastal Erosion, a Case Study for Palm Beach-Azur, Algeria," *Sustainability*, vol. 14, no. 24, pp. 1-12, 2022. [CrossRef] [Google Scholar] [Publisher Link]
[35] Sung-Jae Kim, Weoncheol Koo, and Min-Jae Shin, "Numerical and Experimental Study on a Hemispheric Point-Absorber-Type Wave Energy Converter with a Hydraulic Power Take-Off System," *Renewable Energy*, vol. 135, pp. 1260-1269, 2019. [CrossRef] [Google Scholar] [Publisher Link]
[36] Shaohui Yang et al., "Modelling and Analysis of Inertia Self-Tuning Phase Control Strategy for a Floating Multi-Body Wave Energy Converter," *IET Renewable Power Generation*, 2021. [CrossRef] [Google Scholar] [Publisher Link]
[37] W.E. Cunnnins, The Impulse Response Function and Ship Motion, *DTIC*, 1962. [Google Scholar] [Publisher Link]
[38] T. Francis Ogilvie "Recent Progress Toward the Understanding and Prediction of Ship Motions," *Proceedings of the 5th Symposium on Naval Hydrodynamics*, Bergen, Norway, pp. 3-80, 1964. [Google Scholar]
[39] Frameless Motor for Direct Drive, Alxion, Torque Motors, Permanent Magnet Generators, Resolvers, Servo Drives. [Online]. Available: http://www.alxion.com/products/stk-alternators/
[40] Richard G. Budynas, and J. Keith Nisbett, Shigley's Mechanical Engineering Design, 10th ed., McGraw Hill: New York, NY, USA, 2015. [Google Scholar]
[41] M. López, M. Veigas, and G. Iglesias, "On the Wave Energy Resource of Peru," *Energy Conversion and Management*, vol. 90, pp. 34-40, 2015. [CrossRef] [Google Scholar] [Publisher Link]